Published by Avanti Publishers

Global Journal of Energy Technology Research Updates

ISSN (online): 2409-5818

Seamless Switching Technology of UPQC Based on Improved Power Angle Control

Zhengwei Qu[1], Zhe Shi[1], Yunjing Wang[1], Ahmed Abu-Siada[2], Baona Wang[1] and Haiyan Dong[1,*]

[1]*The Department of Electrical Engineering, Yanshan University, Qinhuangdao 066004, China.*

[2]*School of Electrical Engineering Computing and Mathematical Sciences, Curtin University, Perth, WA 6102, Australia.*

ARTICLE INFO

Article Type: Research Article

Keywords:
Power quality
Seamless switching
Coordinated control
Power angle control
Unified power quality conditioner

Timeline:
Received: September 15, 2021
Accepted: November 05, 2021
Published: December 28, 2021

Citation: Qu Z, Shi Z, Wang Y, Abu-Siada A, Wang B, Dong H. Seamless Switching Technology of UPQC Based on Improved Power Angle Control. Glob J Energ Technol Res Updat. 2021; 8: 54-70.

DOI: https://doi.org/10.15377/2409-5818.2021.08.4

ABSTRACT

This paper presents a novel seamless switching technology between different operating conditions of the Unified Power Quality Conditioner (UPQC) with the energy storage system. Frequent start and stop of the series inverter will cause shock and loss under the conventional control method. Moreover, it is a key issue to achieve seamless switching when the UPQC operating condition changes. This paper proposes an improved power angle control (PAC) method to solve these problems. An agile power angle is calculated by this method under stable operating conditions. This feature enables the series inverter to share the load reactive power with the shunt inverter. On the other hand, both the series and shunt inverters are in an easy-to-switch operating state which can help achieve better seamless switching between different operating conditions. Simulation results show the shunt inverter capacity can be reduced up to 47% due to the reactive power sharing by both the inverters which means the reactive power burden of the shunt inverter is great lightened. It is also found that the switching time is about 300μs faster and the maximum voltage fluctuation amplitude is about 90V smaller under improved PAC than the conventional control method.

*Corresponding Author
Email: dydldhy@163.com
Tel: 13785929164

1. Introduction

With the rapid development of power systems and widespread use of nonlinear electronic equipment, the various issues of power quality (PQ) [1] like voltage swell, sag, interruptions, current and voltage harmonics are becoming a great challenge to the utilities [2]. In order to improve the power quality, static synchronous series compensator (SSSC) [3], static var compensator (SVC) [4], active power filter (APF) [5,6] and dynamic voltage restorer (DVR) [7], etc. are studied. However, most of these devices have a single function and can't achieve coordinated control of power quality. Therefore, a unified power quality conditioner (UPQC) [8] which have multi-function is proposed.

The basic topology of UPQC-based system is shown in Fig. (**1**). It consists of two voltage source inverters which are connected back to back and share a common DC link in between. One inverter acts as a shunt APF ($UPQC_{sh}$), whereas the other as a series APF ($UPQC_{se}$).

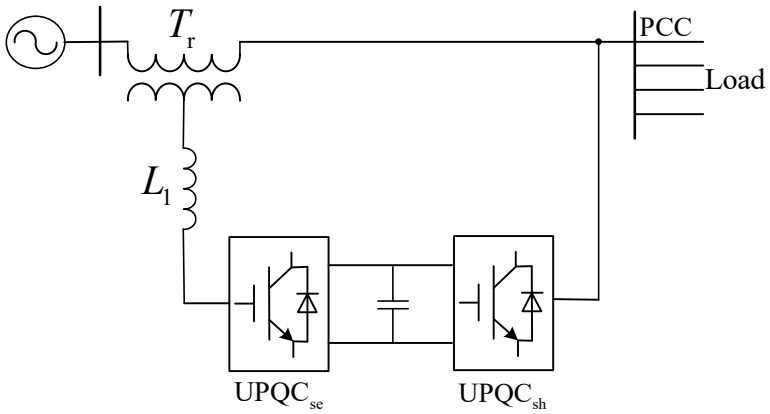

Figure 1: Basic topology of UPQC-based system.

The load-reactive power compensation in most of the UPQC-based power quality compensation applications is done by $UPQC_{sh}$, whereas, the $UPQC_{se}$ is generally utilized to compensate voltage related problems. Power angle control (PAC) [9,10] is widely used in UPQC because it can better utilize the capacity of UPQCse to compensate load-reactive power by introducing a power angle difference between the source and load voltage, making their magnitudes always to be equal.

Many types of research have been done on PAC of UPQC. According to the different power angle δ, the PAC of UPQC can be divided into active power compensation control (UPQC-P) [11], reactive power compensation control (UPQC-Q) [12], UPQC-S control (S for complex power) [13] and minimum energy control (UPQC-VAmin) [14,15]. A comprehensive review of UPQC is reported in [16]. A detailed comparison of design and operational aspects of UPQC-Multiconverter and UPQC-Distributed Generation in [17]. A 3-phase 4-wire UPQC structure is proposed in [18], which has the ability to achieve a dual compensation strategy. A novel nine switch UPQC is used in [19], which reduces the switching stress, less commutation, low losses with less cost. The loss comparison of UPQC-P, UPQC-Q and UPQC-S is proposed in [20]. Three control algorithms based on unit vector technique, single-phase d-q theory and Fourier analysis are applied on single-phase UPQC in [21], and the performance of the three control methods are compared for power factor correction, current and voltage harmonic suppression. Due to the UPQCsh being loaded heavily and the UPQCse being kept idle in steady-state cases, a new coordinated active power sharing control algorithm between shunt and series converters of UPQC is proposed in [22]. However, it ignores the coordinated reactive power control between shunt and series converters and the seamless switching problem of UPQC between different operating conditions.

At present, there is little research about the seamless switching control under different conditions for the UPQC. Thus, this paper proposes an improved PAC algorithm that makes the $UPQC_{se}$ in an easy-to-switch

operating state by calculating an agile power angle under steady conditions. This improved method is also utilized to compensate voltage sag/swell while sharing the load reactive power between $UPQC_{se}$ and $UPQC_{sh}$.

2. The Improved Power Angle Control and Seamless Switching Strategy of UPQC

2.1. Basic Principle of Power Angle Control

Fig. (**2**) shows the system schematic of the UPQC integrated with the battery energy storage system (BESS) at the DC link of back to back connected converters. The main purpose of the UPQC is to transfer the power generated from the BESS to the load and also to improve the voltage and current power quality problems. This paper adopts the UPQC-S control strategy, which combines the advantages of UPQC-P and UPQC-Q. This modified approach is utilized to compensate voltage sag/swell while sharing the load reactive power between two inverters.

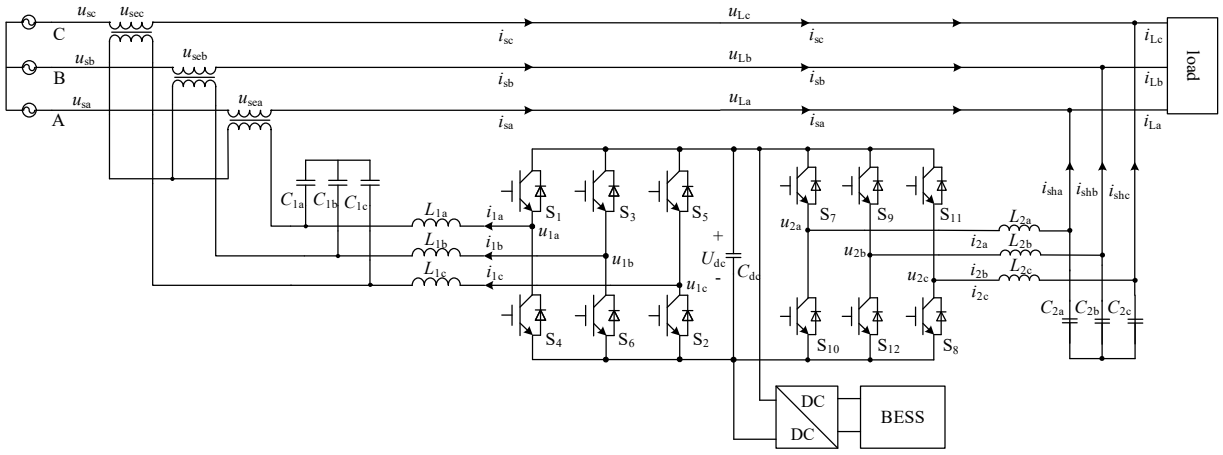

Figure 2: Schematic of three phase UPQC with BESS.

The source voltage may be under three operating conditions: steady, sag and swell. The phasor representation of PAC is shown in Fig. (**3**).

Considering the source voltage $\dot{U}_s$ as the reference phasor, during steady-state $\dot{U}_s$ and the load voltage $\dot{U}_L$ will be at the same magnitude and in-phase.

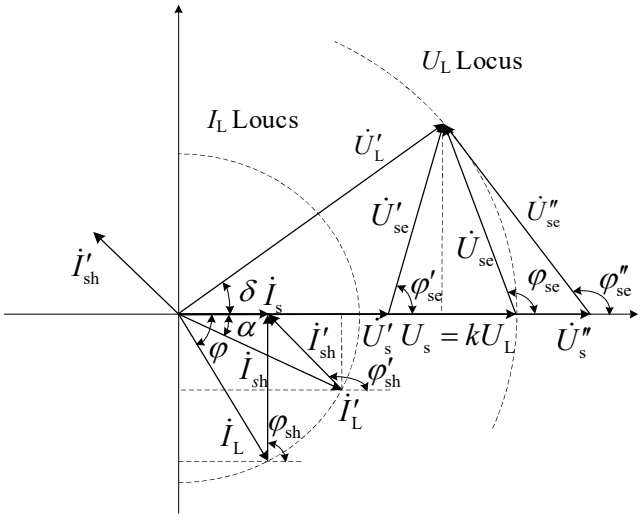

Figure 3: The UPQC compensation phasor diagram based on PAC.

According to Fig. (**3**), a voltage $\dot{U}_{se}$ injected through UPQC$_{se}$ gives a power angle δ boost between $\dot{U}_s$ and resultant load voltage $\dot{U}_L'$ maintaining the same voltage magnitudes. This causes the load current phasor advancement $\dot{I}_L$ to $\dot{I}_L'$ maintain the same load phase angle φ relationship with load voltage. Therefore, the effective load phase angle with respective source voltage boosts from φ to α. The voltage fluctuation factor k, which is defined as the ratio of the instantaneous source voltage to the rated load voltage magnitude, is represented as

$$U_s = kU_L(0.85 \le k \le 1.15) \tag{1}$$

The UPQC$_{se}$ can achieve the following three functions by adjusting the power angle: (a) Keep the magnitude of the load voltage at the desired level; (b) When the voltage sag/swell on the source side, there will be no impact on the load; (c) The load reactive power demand can be shared by UPQC$_{se}$ and UPQC$_{sh}$.

For rated steady state

$$\left|\dot{U}_s\right| = \left|\dot{U}_L\right| = U = x \tag{2}$$

$$\left|I^{'}{}_L\right|\left|\dot{I}_L\right| \tag{3}$$

Fig. (**4**) shows the detailed phasor representation to determine the series compensating voltage.

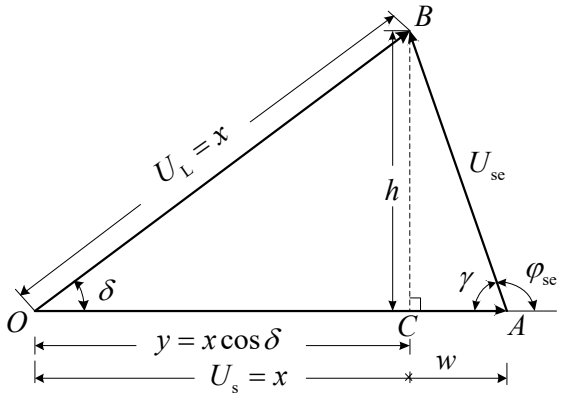

Figure 4: Compensation phasor diagram of UPQC$_{se}$.

From ΔABC (Fig. **4**), we can obtain the magnitude and phase angle of $\dot{U}_{se}$

$$U_{se} = \sqrt{h^2 + w^2} \quad = \sqrt{(x\sin\delta)^2 + [x(1-\cos\delta)]^2} \quad = \sqrt{2}U\sqrt{1+\cos\delta} \tag{4}$$

$$\gamma = tan^{-1}\left(\frac{h}{w}\right) \quad = tan^{-1}\left(\frac{x\sin\delta}{x - x\cos\delta}\right) = tan^{-1}\left(\frac{\sin\delta}{1-\cos\delta}\right) \tag{5}$$

$$\varphi_{se} = 180° - \gamma \tag{6}$$

and the active power and reactive power flow through of UPQC$_{se}$

$$P_{se} = U_{se}I_s\cos\varphi_{se} \quad = -U_{se}I_s\cos\gamma = -(1-\cos\delta)UI\cos\varphi \tag{7}$$

$$Q_{se} = U_{se}I_s\sin\varphi_{se} = UI\sin\delta\cos\varphi \tag{8}$$

where

$$\delta = sin^{-1}\left(\frac{Q_{se}}{P_L}\right) = sin^{-1}\left(\frac{Q_{se}\tan\varphi}{Q_L}\right) \tag{9}$$

where P_L and Q_L are the load active and reactive power, respectively.

Fig. (**5**) represents the detailed phasor representation to determine the shunt compensating current.

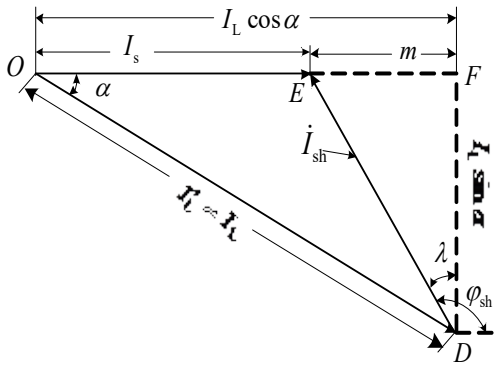

Figure 5: Compensation phasor diagram of UPQC$_{sh}$

From ΔDEF (Fig. **5**), we can obtain the magnitude and phase angle of $\dot{I}_{sh}$

$$I_{sh} = \sqrt{(I_L \sin\alpha)^2 + (I_L \cos\alpha - I_s)^2} \quad = I\sqrt{1 + \cos\varphi - 2\cos\alpha \cdot \cos\varphi} \tag{10}$$

where

$$\alpha = \varphi - \delta \tag{11}$$

$$\lambda = tan^{-1}\left(\frac{m}{I_L \sin\alpha}\right) \quad = tan^{-1}\left(\frac{\cos\alpha - \cos\varphi}{\sin\alpha}\right) \tag{12}$$

$$\varphi_{sh} = 90° + tan^{-1}\left(\frac{\cos\alpha - \cos\varphi}{\sin\alpha}\right) \tag{13}$$

and the active power and reactive power flow through of UPQC$_{sh}$

$$P_{sh} = U_L I_{sh} \sin(\lambda - \delta) \quad = UI[\sin\delta\,(\cos\alpha - 1) - \cos\delta \sin\alpha] \tag{14}$$

$$Q_{sh} = U_L I_{sh} \cos(\delta - \lambda) \quad = UI[\cos\delta \sin\alpha + \sin\delta\,(\cos\lambda - 1)] \tag{15}$$

2.2. The Improved Power Angle Control

Average reactive power distribution control was proposed in [23], in which the UPQC$_{se}$ and UPQC$_{sh}$ are controlled to provide one-half of the load reactive power demand, respectively. With this method, UPQC$_{se}$ is in an agile state and UPQC$_{se}$ can rapidly respond when a sag or swell occurs in the system. Based on this method, an improved PAC strategy is proposed, which can determine an agile power angle δ_0 according to whether the capacity of the UPQC$_{se}$ meets the load reactive power demand. The principle for determining the agile power angle is as follows:

Let $Q_{se,max}$ be the maximum load-reactive power capacity of UPQC$_{se}$.

1) If the load-reactive power demand is less than $Q_{se,max}$ ($Q_{se,max} \geq Q_L$), let Q_L replace Q_{se} in equation (9) and take one-half of the calculated power angle.
2) If the load-reactive power demand is more than $Q_{se,max}$ ($Q_{se\_max} < Q_L$), let Q_{se_max} replace Q_{se} in equation (9) and take one-half of the calculated power angle.

Through the above principles we can obtain δ_0.

$$\delta_0 = \begin{cases} \frac{1}{2} sin^{-1}(tan\,\varphi)\,, & Q_{se,max} \geq Q_L \\ \frac{1}{2} sin^{-1}\left(\frac{Q\,tan\,\varphi_{se,max}}{Q_L}\right) & \end{cases} \tag{16}$$

According to equation (16), when the load power angle φ is determined, the agile power angle δ_0 is also determined.

On the other hand, consider that the UPQC system is already working under improved PAC method, i.e., both the inverters are compensating the load reactive power and the $UPQC_{se}$ is controlled in an agile state, so seamless switching of the device between different conditions can be realized when there is sag or swell problem with the source voltage. Under improved PAC, the power angle δ is changed to δ_0 in Figs. (**4** and **5**). The new detailed phasor representation is shown in Figs. (**6** and **7**).

For $UPQC_{se}$ (see Fig. **6**).

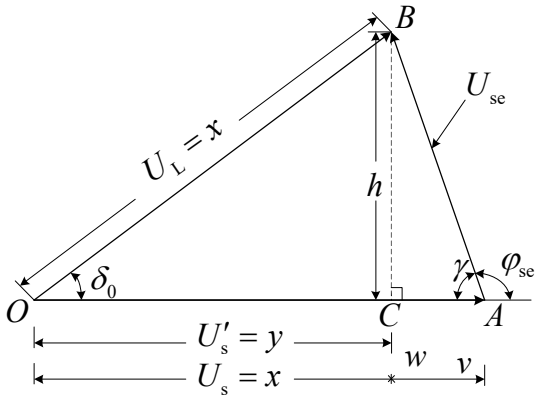

Figure 6: Phasor representation of the $UPQC_{sh}$ under-voltage steady condition.

from equation (4),

$$U_{se} = \sqrt{2}U\sqrt{1 - cos\ \delta_0} \tag{17}$$

from equation (6),

$$\varphi_{se} = 180° - tan^{-1}\left(\frac{sin\ \delta_0}{1 - cos\ \delta_0}\right) \tag{18}$$

For active and reactive power

$$P_{se} = -UI(1 - cos\ \delta_0)\ cos\ \varphi \tag{19}$$

$$Q_{se} = U_{se}I_s\ sin\ \varphi_{se} = UI\ sin\ \delta_0\ cos\ \varphi \tag{20}$$

For $UPQC_{sh}$ (see Fig. **7**)

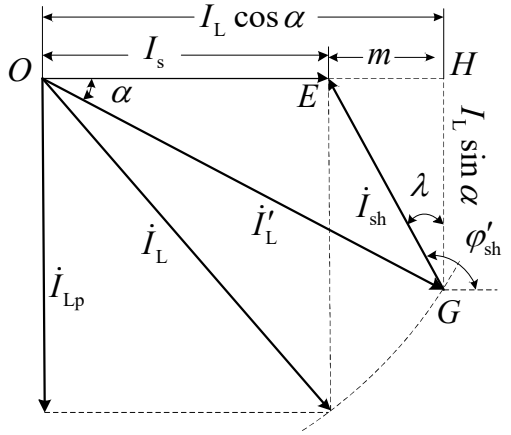

Figure 7: Phasor representation of the $UPQC_{sh}$ under-voltage steady condition.

from equation (11),

$$I_{sh}=I\sqrt{(sin\,\alpha)^2+(cos\,\alpha-cos\,\varphi)^2} \tag{21}$$

from equation (13),

$$\varphi_{sh}=90°+tan^{-1}\left(\frac{cos\,\alpha-cos\,\varphi}{sin\,\alpha}\right) \tag{22}$$

For active and reactive power

$$P_{sh}=U_L I_{sh}\sin\mu=UI(1-cos\,\delta_0)\,cos\,\varphi \tag{23}$$

$$Q_{sh}=U_L I_{sh}\,cos\,\mu=UI(sin\,\varphi-sin\,\delta_0\,cos\,\varphi) \tag{24}$$

Table 1: Comparison with an existing method.

φ	Traditional Control		Average Distribution Control			Improved PAC		
	Q_{se}(p.u.)	Q_{sh}(p.u.)	Q_{se}(p.u.)	Q_{sh}(p.u.)	P_h(p.u.)	Q_{se}(p.u.)	Q_{sh}(p.u.)	P_h(p.u.)
25°	0	0.4226	0.2113	0.2113	0.0264	0.2177	0.2049	0.0250
28°	0	0.4695	0.2347	0.2347	0.0345	0.2443	0.2252	0.0318
30°	0	0.5	0.25	0.25	0.0407	0.2623	0.2377	0.0369
32°	0	0.5299	0.2607	0.2607	0.0478	0.2808	0.2491	0.0425

It can be seen from equations (19) and (23) that, for ideal conditions, without any losses, the active power consumed by $UPQC_{se}$ should be equal to the active power fed back by $UPQC_{sh}$ and hence, the source current would be constant. Table **1** compares the results of the traditional control, average distribution control and the improved PAC. Where P_h is active power circulation.

According to the analysis of Table **1**, the seamless switching strategy by improved PAC has obvious advantages in sharing load reactive power of $UPQC_{se}$ and reducing the overall capacity of UPQC. At the same time, it does not increase the capacity of $UPQC_{se}$, but only makes full utilization of the existing capacity of UPQC, which is helpful to reduce the cost. The active power circulation between UPQC and the line is also reduced compared with the traditional control. More importantly, $UPQC_{se}$ has always been in an agile working state, which reduces the shock and loss problem caused by frequent start and stops of $UPQC_{se}$ in the traditional control. In this article, the method of improved PAC can avoid the risk of the over-limiting capacity of the compensator and ensure that it operates in the most sensitive switching state.

2.3. The Improved Power Control Approach Under Voltage Sag/Swell Condition

If a voltage sag/swell condition occurs on the system, $UPQC_{se}$ and $UPQC_{sh}$ should keep supplying the load reactive power, as they were steady. Irrespective of the variation in the source voltage the $UPQC_{se}$ should maintain the same agile power angle δ_0 between both the source and load voltages. However, if the load changes during the voltage sag/swell condition, the $UPQC_{se}$ will give a differentδ_0. The size of the new δ_0 angle would depend on the increase or decrease in load reactive power.

The BESS will be working no matter what the voltage sag or swell and can absorb or provide active power to maintain constant output current. In order to achieve seamless switching between different conditions, always maintain the agile power angle δ_0 of constant.

2.3.1 Under Voltage Sag Condition

Fig. (**8**) represents the phasor diagram to calculate the injected voltage magnitude and phase angle of $UPQC_{se}$.

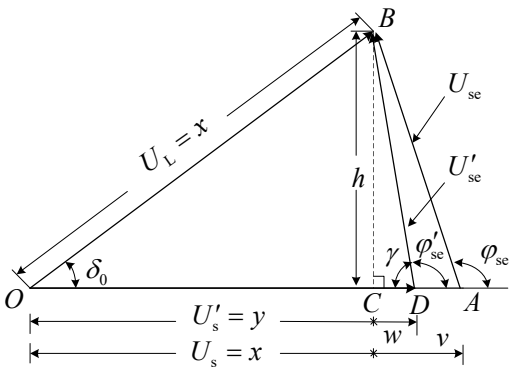

Figure 8: Phasor representation of the UPQC$_{se}$ under voltage sag condition.

To calculate the magnitude and phase angle of $\dot{U}'_{se}$, from ΔBCD in Fig. (**8**).

$$U'_{se} = U\sqrt{1 + k^2 - 2k\cos\delta_0} \tag{25}$$

$$\varphi'_{se} = 180° - tan^{-1}\left(\frac{\sin\delta_0}{k - \cos\delta_0}\right) \tag{26}$$

where $0.85<k<1$

For active and reactive power

$$P'_{se} = U'_{se}I'_s\cos\varphi'_{se} \ = -U'_{se}I'_s\cos\gamma = -UI\cos\varphi\left(1 - \frac{1}{k}\cos\delta_0\right) \tag{27}$$

$$Q'_{se} = \frac{1}{k}UI\sin\delta_0\cos\varphi \tag{28}$$

Fig. (**9**) represents the phasor diagram to calculate the injected current magnitude and phase angle of UPQC$_{sh}$.

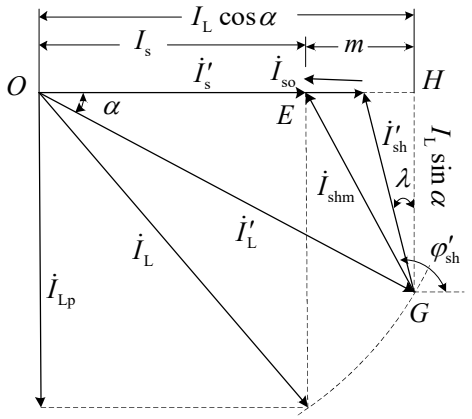

Figure 9: Phasor representation of the UPQC$_{sh}$ under voltage sag condition.

To calculate the magnitude of the phase angle of $\dot{I}'_{sh}$, from ΔGEH in Fig. (**9**).

$$I'_{sh} = I\sqrt{1 + \frac{1}{k^2}\cos^2\varphi - \frac{2}{k}\cos\alpha\cos\varphi} \tag{29}$$

$$\varphi'_{sh} = 90° + tan^{-1}\left(\frac{k\cos\alpha - \cos\varphi}{k\sin\alpha}\right) \tag{30}$$

For active and reactive power

$$P'_{sh} = UI\left[\left(cos\,\alpha - \frac{1}{k}cos\,\varphi\right)cos\,\delta_0 - sin\,\alpha\,sin\,\delta_0\right] \tag{31}$$

$$Q'_{sh} = UI\left[sin\,\alpha\,cos\,\delta_0 + \left(cos\,\alpha - \frac{1}{k}cos\,\varphi\right)sin\,\delta_0\right] \tag{32}$$

The BESS is utilized to control the $UPQC_{sh}$ output constant power, and the output source current is also constant. In this case, the current output by the $UPQC_{sh}$ $\dot{I}_{shm}$ is made up of the output current $\dot{I}_{so}$ by the BESS and the compensation current $I^{'}{}_{sh}$ required for the operation of the device, we can get

$$\dot{I}_{shm} = \dot{I}_{so} + I^{'}{}_{sh} \tag{33}$$

2.3.2. Under Voltage Swell Condition

Under voltage swell condition, the $UPQC_{se}$ injected voltage magnitude and its phase angle are shown in Fig. (**10**).

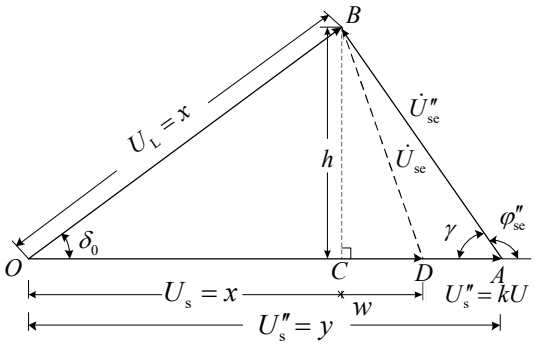

Figure 10: Phasor representation of the $UPQC_{se}$ under-voltage swell condition.

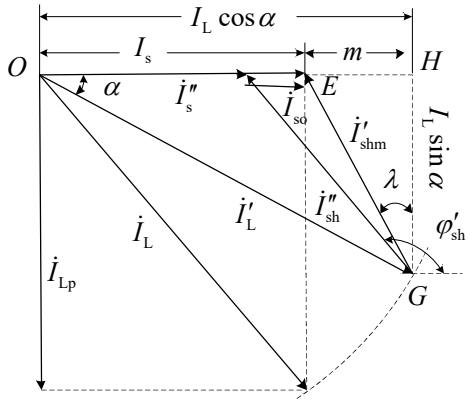

Figure 11: Phasor representation of the $UPQC_{se}$ under-voltage swell condition.

To calculate the magnitude and phase angle of $\dot{U}''_{se}$, from ΔABC in Fig. (**10**).

$$U''_{se} = U\sqrt{1 + k^2 - 2k\,cos\,\delta_0} \tag{34}$$

$$\gamma = tan^{-1}\left(\frac{h}{y - x + w}\right) = tan^{-1}\left(\frac{sin\,\delta_0}{k - cos\,\delta_0}\right) \tag{35}$$

Therefore,

$$\varphi_{se}^{''} = 180° - tan^{-1}\left(\frac{sin\,\delta_0}{k - cos\,\delta_0}\right) \tag{36}$$

where 1<k<1.15

For active and reactive power

$$P_{se}^{''} = U_{se}^{''} I_s^{''} cos\,\varphi_{se}^{''} = -U_{se}^{''} I_s^{''} cos\,\gamma = -UI\left(1 - \frac{1}{k} cos\,\delta_0\right) cos\,\varphi \tag{37}$$

$$Q_{se}^{''} = U_{se}^{''} I_s^{''} sin\,\varphi_{se}^{''} = \frac{1}{k} UI\,sin\,\delta_0\,cos\,\varphi \tag{38}$$

The UPQC$_{sh}$ injected current magnitude and its phase angle are shown in Fig. (**11**).

To calculate the magnitude and phase angle of $\dot{I}_{sh}^{''}$, from ΔEGH in Fig. (**11**).

$$I_{sh}^{''} = I\sqrt{1 + \frac{1}{k^2} cos^2\,\varphi - \frac{2}{k} cos\,\alpha\,cos\,\varphi} \tag{39}$$

$$\varphi_{sh}^{''} = 90° + \lambda = 90° + tan^{-1}\left(\frac{cos\,\alpha - cos\,\varphi}{sin\,\alpha}\right) \tag{40}$$

For active and reactive power

$$P_{sh}^{''} = UI\left[\left(cos\,\alpha - \frac{1}{k} cos\,\varphi\right) cos\,\delta_0 - sin\,\alpha\,sin\,\delta_0\right] \tag{41}$$

$$Q_{sh}^{''} = UI\left[sin\,\alpha\,cos\,\delta_0 + \left(cos\,\alpha - \frac{1}{k} cos\,\varphi\right) sin\,\delta_0\right] \tag{42}$$

In this case, the current $\dot{I}_{shm}'$ by the UPQC$_{sh}$ is made up of the output current $\dot{I}_{so}'$ by the BESS and the compensation current $I^{''}{}_{sh}$ required for the operation of the device, which we can get.

$$\dot{I}_{shm}' = \dot{I}_{so}' + I_{sh}'' \tag{43}$$

2.4. UPQC$_{se}$ Controller

Under voltage steady conditions, the value of the agile power angle δ_0 is determined. With standard mathematical computation the required UPQC$_{se}$ injected voltage magnitude and its phase angle can be calculated by (17) and (18) respectively. Fig. (**12**) shows the UPQC$_{se}$ injected reference voltage $U_{sea}^*, U_{seb}^*, U_{sec}^*$. The sinusoidal and cosine signals, at unity magnitude, from the phase-locked loop (PLL) are used to maintain the synchronization between the generated reference signal and the source voltage. Similarly, with $\pm 120°$ phase angle differences the reference signals for the other two phases are generated.

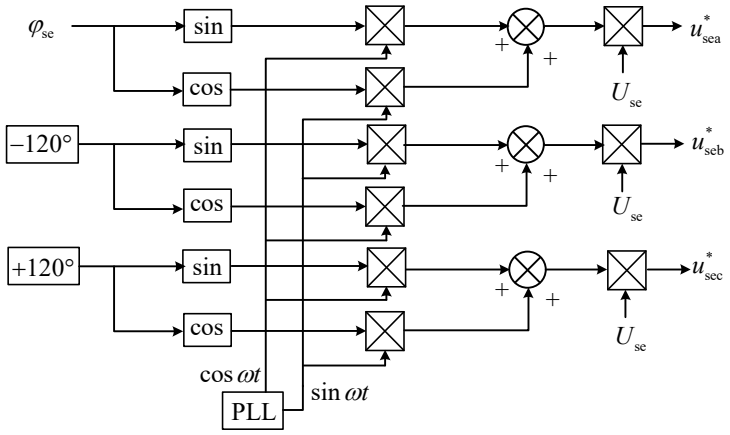

Figure 12: The UPQC$_{se}$ injected voltage reference signals.

The control schematic for the UPQC$_{se}$ is shown Fig. (**13**). Based on p-q theory, the U^*_{sed} and U^*_{seq} are calculated. In order to compensate voltage harmonic, the required voltage harmonic compensation value is extracted by using a low-pass filter (LPF), which is used as the UPQC$_{se}$ reference voltage signals. In addition, a voltage feedforward compensation method is utilized to enhance dynamic performance of system.

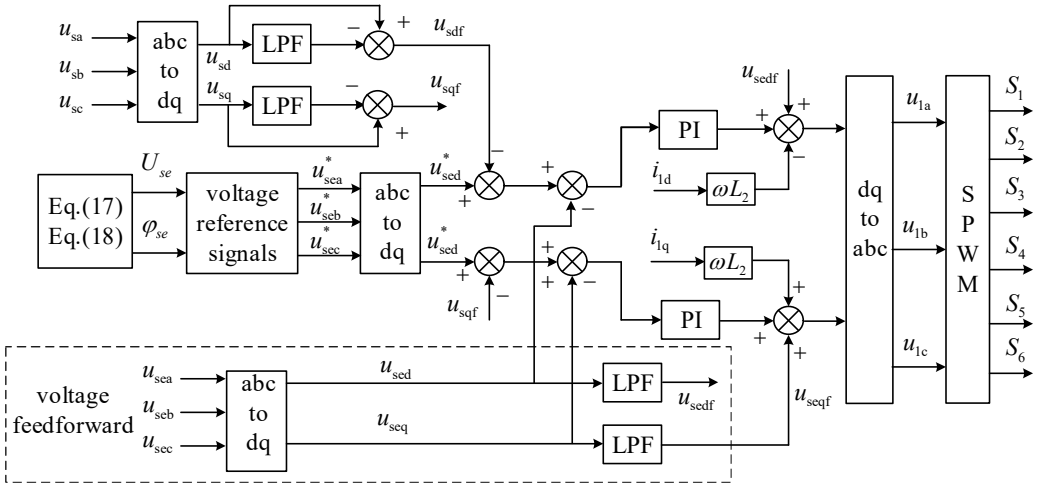

Figure 13: Control schematic for the UPQC$_{se}$.

2.5. UPQC$_{sh}$ Controller

The control principle of UPQC$_{sh}$ is similar to the UPQC$_{se}$, the required UPQC$_{sh}$ injected current magnitude and its phase angle are calculated by (21) and (22) respectively. Figs. (**14** and **15**) shows the UPQC$_{sh}$ injected current reference signals $i^*_{sha}, i^*_{shb}, i^*_{shc}$ and control schematic for the UPQC$_{sh}$, respectively.

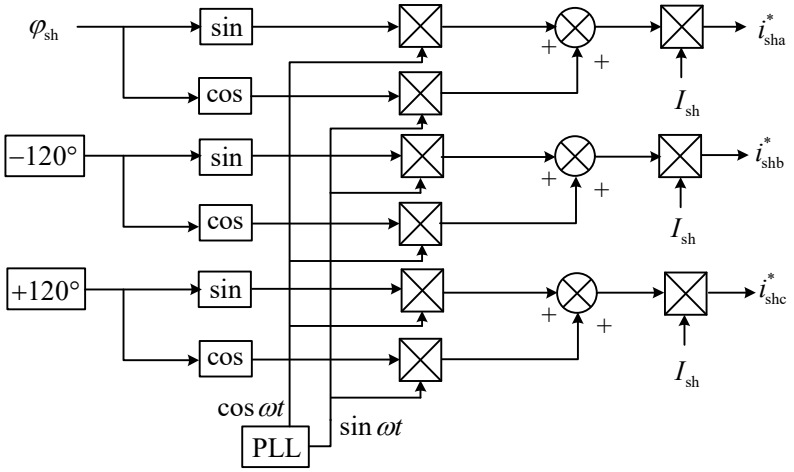

Figure 14: The UPQC$_{sh}$ injected voltage reference signals.

2.6. Energy Storage System Controller

In this paper, the energy storage system utilises voltage and current double closed-loop control to improve the ability of bus voltage self-regulation. The power coordination control schematic of the energy storage system is shown in Fig. (**16**).

where u^*_{dc} is the DC bus reference value, u_{dc} is the DC bus voltage measurement value, i^*_{cn} is the reference current value, i_{cn} is the actual output current value of the energy storage unit.

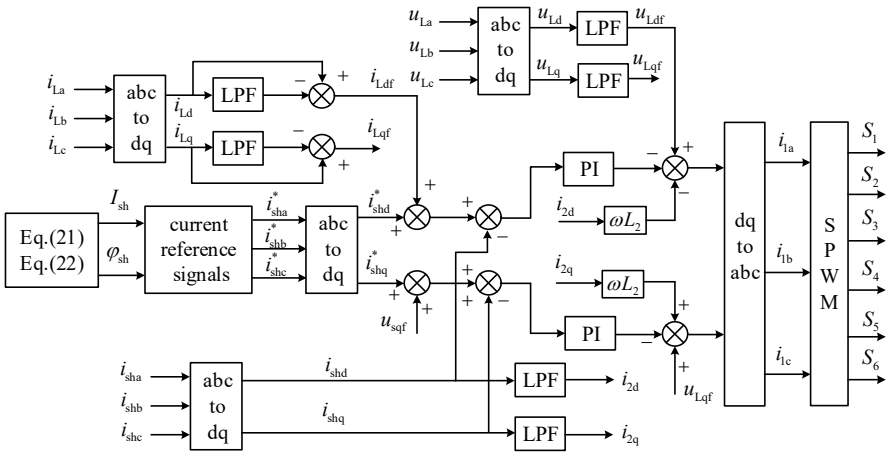

Figure 15: Control schematic for the $UPQC_{sh}$.

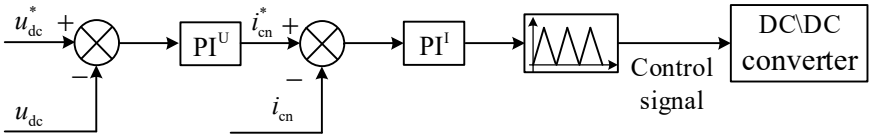

Figure 16: Energy storage system control.

3. Results and Discussion

The performance of the improved PAC and seamless switching strategy has been verified by simulation. The main parameters are shown in Table **2**.

Table 2: UPQC parameters.

Name	Value	Name	Value
rms utility voltage	380V	$UPQC_{sh}$ filtering inductances	L_1 = 7.8mH
Utility grid frequency	f_s = 50Hz	$UPQC_{sh}$ filtering capacitances	C_1 = 1.16μF
SPWM switching frequency (series/shunt inverter)	f_{sw} = 16.7kHz	$UPQC_{se}$ filtering inductances	L_2 = 2mH
Capacitance of the dc-bus	C_{dc} = 6600μF	$UPQC_{sh}$ and $UPQC_{se}$ capacity	10kVA
DC bus voltage	U_{dc} = 800V	Load capacity	10kVA(P=8.66kW，Q=5kvar)
Maximum compensation voltage	U_{semax} = 207.35V	$UPQC_{se}$ filtering capacitances	C_2 = 5μF
Transformer ratio	N = 2		

3.1. Steady-State Operating Conditions

For a rated steady condition, the reactive power sharing feature of $UPQC_{se}$ and $UPQC_{sh}$ has been evaluated by MATLAB/SIMULINK. Figs. (**17–22**) shows the simulation results with the proposed control in this paper.

As shown in Fig. (**17**), the unity power factor is achieved. It can be seen from Fig. (**18**) that the magnitude of the load and the source voltage is maintained at the desired level, but the phase angle is different. Fig. (**19**) shows the waveform of the DC bus voltage. The magnitude of the DC bus voltage is basically maintained at 800V, with only slight fluctuations at the beginning. As shown in Figs. (**20** and **21**), the reactive power output by $UPQC_{se}$ and $UPQC_{sh}$ is 2.623 kvar and 2.377 kvar, respectively. Both the $UPQC_{se}$ and $UPQC_{sh}$ supply the load-reactive power demand. Under the improved PAC, the $UPQC_{sh}$ capacity can be reduced up to 47%. The $UPQC_{se}$ outputs more

reactive power than the average reactive power control method. There is a minute active power exchange between $UPQC_{se}$ and $UPQC_{sh}$, with a value of 0.407kW (about 0.45% of the system capacity). It can be seen from Fig. (**22**) that the reactive power output by $UPQC_{se}$ is always greater than the reactive power output by $UPQC_{sh}$. It is also found that the improved PAC can make full use of the existing capacity of $UPQC_{se}$ and reduce the reactive power burden of $UPQC_{sh}$. Under steady operating conditions, $UPQC_{se}$ and $UPQC_{sh}$ are controlled in an easy-to-switch operating station, getting ready for seamless switching between different operating conditions.

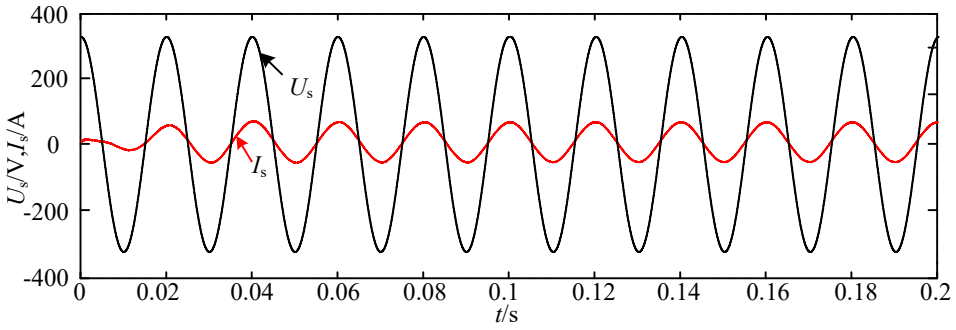

Figure 17: Source voltage and current waveforms under steady-state condition.

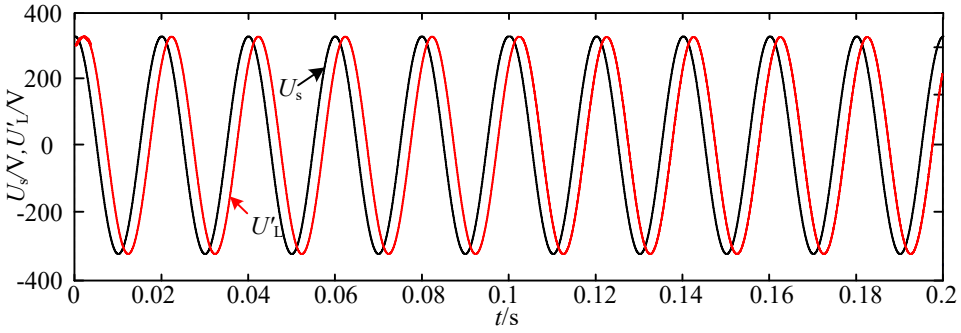

Figure 18: Source and load voltage waveforms under steady state condition.

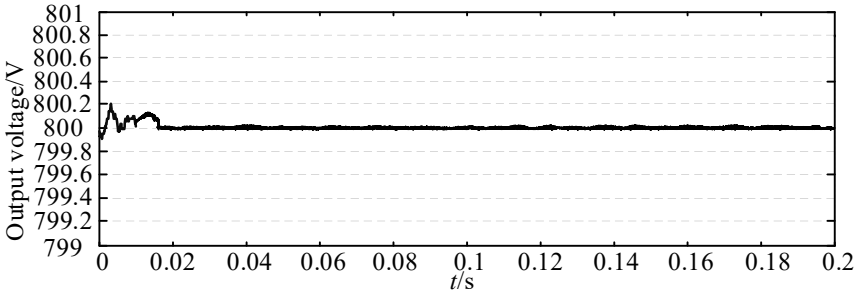

Figure 19: DC bus voltage waveform.

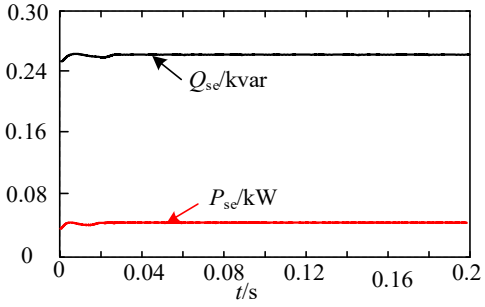

Figure 20: Active and reactive power waveforms of $UPQC_{se}$

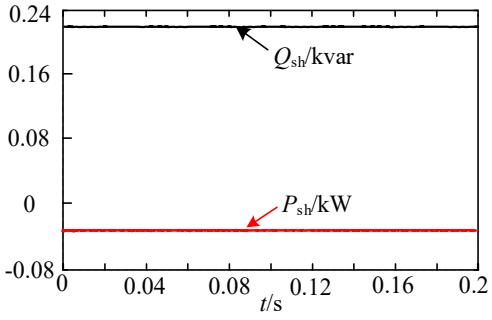

Figure 21: Active and reactive power waveforms of UPQC$_{sh}$.

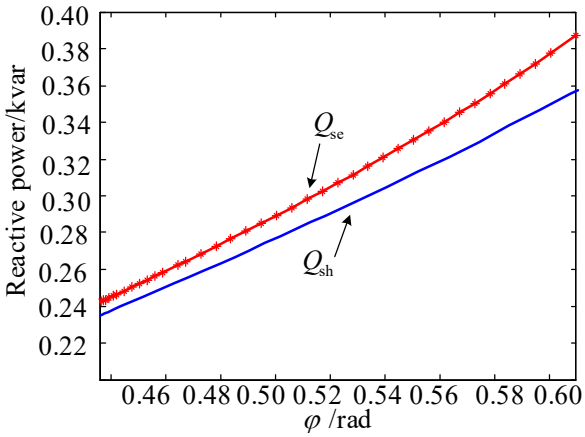

Figure 22: Reactive power of UPQC$_{se}$ and UPQC$_{sh}$.

3.2. Seamless Switching between Different Working Conditions

Fig. (**23-27**) shows the simulation results for the proposed seamless switching control strategy under voltage sag and swell conditions. Before time $t_1 = 0.1s$, the UPQC system is working under steady-state conditions, compensating the load reactive power using UPQC$_{se}$ and UPQC$_{sh}$. At the time $t_1 = 0.1s$, a sag of 15% is introduced on the system (sag last till time $t = 0.2s$). Between the time period $t = 0.2s$ and $t = 0.3s$, the system is again in the steady-state. A swell of 15% is imposed on the system for a duration of $t_2 = 0.3 - 0.4s$.

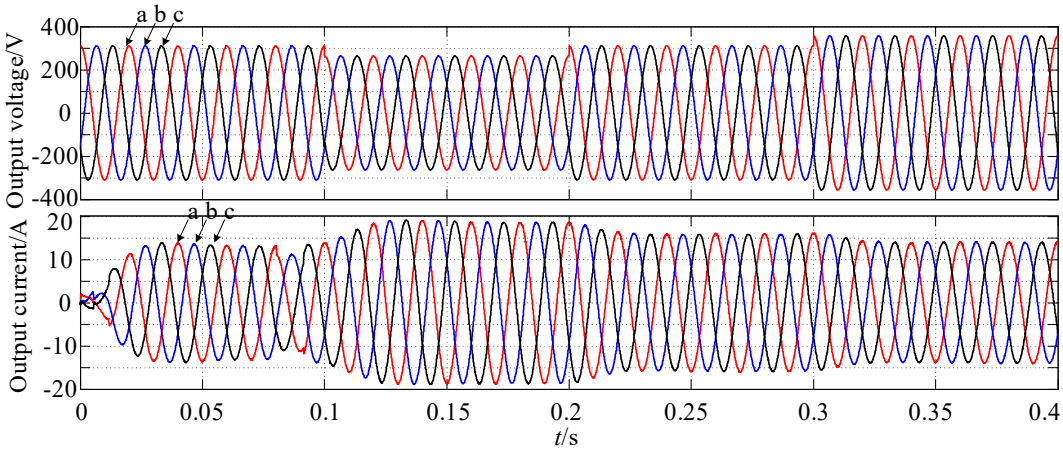

Figure 23: Source voltage and current waveforms.

As shown in Fig. (**23**), the system is operated under the unit power factor. In order to maintain the active power balance in the system, the source current increases during the voltage sag and reduces during the swell condition. From Fig. (**24**), the load voltage profile is maintained at the desired level irrespective of voltage sag (decrease) or swell (increase) in the source voltage magnitudes. It can be seen from Fig. (**25**) that the reactive power output by

$UPQC_{se}$ increases during voltage sag and decreases during voltage swell, while the reactive power output by $UPQC_{sh}$ decreases during voltage sag and increases during voltage swell. $UPQC_{se}$ and $UPQC_{sh}$ can coordinate the power output and realize seamless switching between different states. Figures (**26** and **27**) shows the partially enlarged waveform of the proposed control and the conventional control method, respectively. It can be observed that the switching time is about 700μs, the maximum voltage amplitude during the switching process is about 85V, and has a smaller ripple voltage under the improved PAC method. However, when using the conventional control method, the switching time is about 1000μs, and the maximum voltage amplitude during the switching process is about 175V and has a larger ripple voltage. The switching time under improved PAC is about 300μs faster than the conventional control. Furthermore, the maximum voltage fluctuation amplitude during the switching process under improved PAC is about 90V smaller than the conventional control. Thus, the improved PAC can realize seamless switching of the UPQC system between different operating conditions, and improve the dynamic performance of the system.

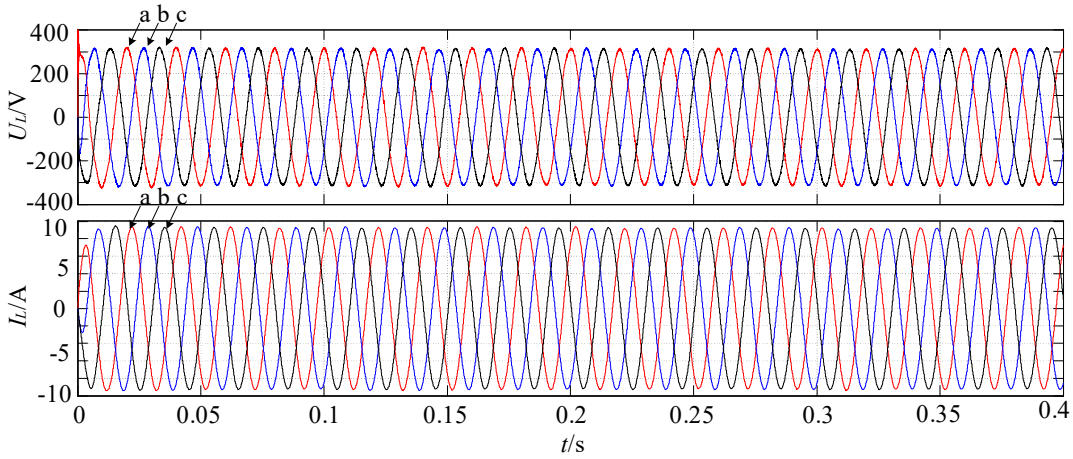

Figure 24: Load voltage and current waveforms.

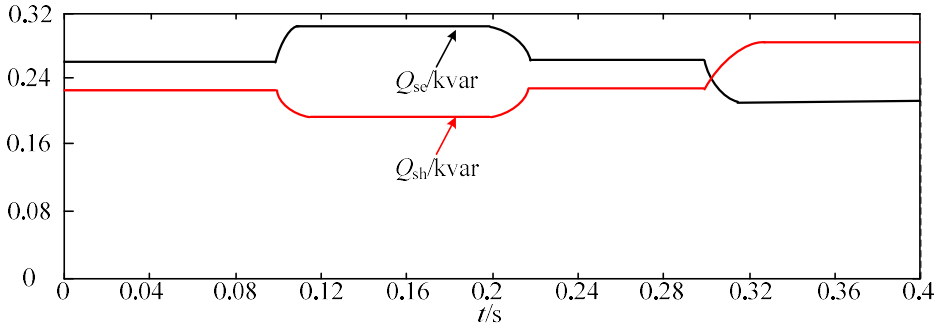

Figure 25: $UPQC_{se}$ and $UPQC_{sh}$ reactive power waveforms.

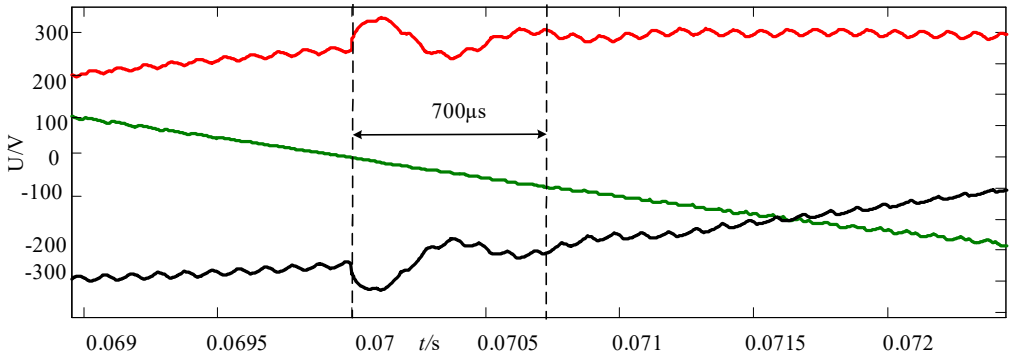

Figure 26: Partial enlarged waveform of source voltage with the proposed control at switching time.

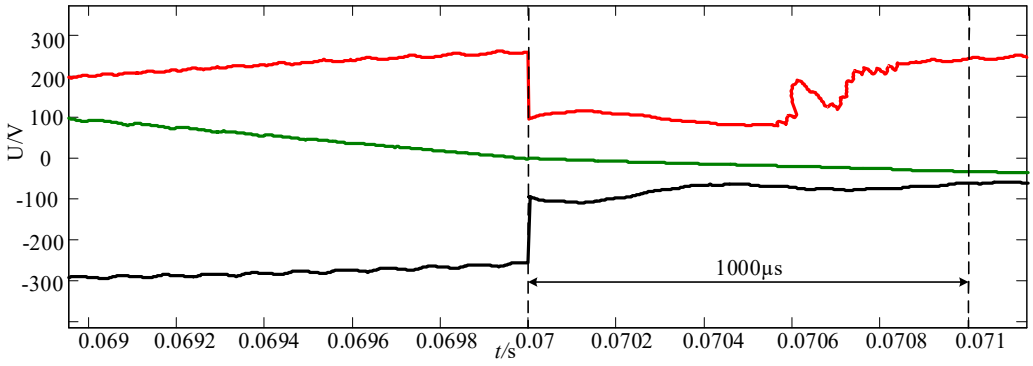

Figure 27: Partially enlarged waveform of source voltage with the conventional control at switching time.

4. Conclusion

In this paper, an improved PAC method of UPQC is proposed. The presented method is mathematically formulated and analyzed for voltage sag and swell conditions. The comprehensive equations for improved PAC can be utilized to estimate the required series injection voltage and the shunt compensating current (magnitude and phase angle). The significant advantages of the proposed method are as follow: 1) alleviates the shock and loss problems caused by frequent start and stop of $UPQC_{se}$; 2) makes better utilization of $UPQC_{se}$ and reduce the burden on the $UPQC_{sh}$. Simulation results show that the $UPQC_{sh}$ capacity is reduced up to 47%; 3) better seamless switching between different operating conditions. Simulation results show that switching time is about 300μs faster and the maximum voltage fluctuation amplitude is about 90V smaller than the conventional control. Future work may include experimental validation of the method used in this work.

References

[1] Paramanik S, Sarker K, Chatterjee D, Goswami SK. Smart Grid Power Quality Improvement Using Modified UPQC. Devices for Integrated Circuit (DevIC). 2019; 356-360. https://doi.org/10.1109/DEVIC.2019.8783704

[2] Bhosale SS, Bhosale YN, Chavan UM, Malvekar SA. Power Quality Improvement by Using UPQC: A Review. International Conference on Control, Power, Communication and Computing Technologies (ICCPCCT). 2018; 375-380. https://doi.org/10.1109/ICCPCCT.2018.8574264

[3] Gita K, Kumar A. SSSC Incorporation in Power System Network for Security Analysis. Uttar Pradesh Section International Conference on Electrical, Electronics and Computer Engineering (UPCON). 2020; 1-6. https://doi.org/10.1109/UPCON50219.2020.9376530

[4] Kecojević K, Lukačević O, Ćalasan M, Mujović S. Minimizing active power losses by incorporating Static Var Compensator (SVC) device into the power system. International Conference on Information Technology (IT). 2020; 1-4. https://doi.org/10.1109/IT48810.2020.9070623

[5] Marcu M, Popescu F, Niculescu T, Pana L, Handra AD. Simulation of power active filter using instantaneous reactive power theory. International Conference on Harmonics and Quality of Power (ICHQP). 2014; 581-585. https://doi.org/10.1109/ICHQP.2014.6842783

[6] Fischer GdS, Mengatto A, Kremer LG, Mezaroba M. A Control Strategy for a Series APF With Critical-Load-Bus Voltage Feedback That Avoids Injection Transformer Saturation. IEEE Transactions on Industry Applications. 2019; 55(3): 2290-2299. https://doi.org/10.1109/TIA.2018.2886769

[7] Tu C, Guo Q, Jiang F et al. Dynamic Voltage Restorer With an Improved Strategy to Voltage Sag Compensation and Energy Self-Recovery. CPSS Transactions on Power Electronics and Applications. 2019; 4(3): 219-229, doi:10.24295/ CPSSTPEA.2019.00021 https://doi.org/10.24295/CPSSTPEA.2019.00021

[8] Muneer V, Sukumaran J, Bhattacharya A. Investigation on reduced DC link voltage based UPQC for harmonic compensation under unbalanced load. International Conference on Technological Advancements in Power and Energy. 2017; 1-6. https://doi.org/10.1109/TAPENERGY.2017.8397336

[9] Kimkaew N, Santiprapan P. Performance Comparison of Switching Techniques for Unified Power Quality Conditioner. International Electrical Engineering Congress (iEECON). 2021; 9-12. https://doi.org/10.1109/iEECON51072.2021.9440268

[10] Khadkikar V, Chandra A. A New Control Philosophy for a Unified Power Quality Conditioner (UPQC) to Coordinate Load-Reactive Power Demand Between Shunt and Series Inverters. IEEE Transactions on Power Delivery. 2008; 23(4): 2522-2534. https://doi.org/10.1109/TPWRD.2008.921146

[11] Naidu NKS, Gooi HB, Yi T, et al. Coordinated active power control between shunt and series converters of UPQC for distributed generation applications. Annual Conference of the IEEE Industrial Electronics Society. 2016; 3697-3702. https://doi.org/10.1109/IECON.2016.7793071

[12] Saicharan K, Gupta AR. Allocation of UPQC in Overloaded Mesh Distribution System with Battery Charging Load. IEEE International Conference on Measurement, Instrumentation, Control and Automation (ICMICA). 2020; 1-5. https://doi.org/10.1109/ICMICA48462.2020.9242788

[13] Khadkikar V, Chandra A. UPQC-S: A Novel Concept of Simultaneous Voltage Sag/Swell and Load Reactive Power Compensations Utilizing Series Inverter of UPQC. IEEE Transactions on Power Electronics. 2011; 26(9): 2414-2425, https://doi.org/10.1109/TPEL.2011.2106222

[14] Ye J, Gooi HB, Zhang X, Wang B, Manandhar U. Two-Level Algorithm for UPQC Considering Power Electronic Converters and Transformers. IEEE Applied Power Electronics Conference and Exposition (APEC). 2019; 3461-3467. https://doi.org/10.1109/APEC.2019.8722007

[15] Hasan M, Singh B, Ansari AQ. An approach to minimize the VA size of UPQC-S and its performance comparison. IEEMA Engineer Infinite Conference (eTechNxT). 2018; 1-5. https://doi.org/10.1109/ETECHNXT.2018.8385344

[16] Wanjari RA, Savakhande VB, Chewale MA, Sonawane PR, Khobragade RM. A Review on UPQC for Power Quality Enhancement in Distribution System. International Conference on Current Trends towards Converging Technologies (ICCTCT). 2018: 1-7. https://doi.org/10.1109/ICCTCT.2018.8550918

[17] Karelia N, Sant AV, Pandya V. Comparison of UPQC Topologies for Power Quality Enhancement in Grid Integrated Renewable Energy Sources. IEEE 16th India Council International Conference (INDICON). 2019: 1-4. https://doi.org/10.1109/INDICON47234.2019.9029108

[18] Modesto RA, Silva SAO, Oliveira AA. Three-phase four-wire unified power quality conditioner structure with independent grid current control and reduced dc-bus voltage operating with inverted/dual compensating strategy. International Transactions on Electrical Energy Systems. 2020; 30(6): https://doi.org/10.1002/2050-7038.12380

[19] Vijayasamundiswary S, Baskaran J. A novel approach to nine switch unified power quality conditioner for power quality improvement. International Conference on Innovative Research in Electrical Sciences (IICIRES). 2017; 1-5. https://doi.org/10.1109/IICIRES.2017.8078291

[20] Yadav SK, Patel A, Mathur HD. Comparison of Power Losses for Different Control Strategies of UPQC. IEEE 9th Power India International Conference (PIICON). 2020; 1-6. https://doi.org/10.1109/PIICON49524.2020.9113005

[21] Pal Y, Swarup A, Singh B. Comparison of three control algorithms for single-phase UPQC. International Conference on Energy, Automation and Signal. 2011: 1-5. https://doi.org/10.1109/ICEAS.2011.6147086

[22] Feng X, Zhang Z, Ma W, Zhang L. UPQC coordinated control strategy with circulating active power. International Conference on Information Science, Electronics and Electrical Engineering. 2014; 3: 1825-1829. https://doi.org/10.1109/InfoSEEE.2014.6946237

[23] Feng X, Wei T, Qi Z. Coordinated Control Strategy of power flow in Voltage Quality Conditioner. Power System Technology. 2013; 37(01): 218-223 (in Chinese).